



A high oxidase-like activity, bimetallic single-atom nanozyme FeCe/NC prepared by FeCe-ZIF-8 approach for sensing tannic acid in tea

Xingyu Zhu, Chong Chen, Dou Che, Hui Yan*

School of Biotechnology, Jiangsu University of Science and Technology, Zhenjiang 212100, China

ARTICLE INFO

Keywords:

Single-atom nanozymes
Oxidase-like
Bimetallic nanozymes
FeCe/NC
Tannic acid
Biosensor

ABSTRACT

To improve the activity of single-atom nanozymes (SAzymes) for applications in food analysis, a new bimetal SAzyme FeCe/NC was developed. Its oxidase-like activity is 40% higher than that of single metal SAzyme Fe/NC. Based on a series of characterization investigations, the catalytic mechanism is that it directly catalyzed O_2 to generate $\bullet OH$, $O_2^{\bullet -}$ and 1O_2 . It could directly catalyze oxidation 3,3',5,5'-tetramethylbenzidine (TMB) to blue oxTMB, thereunder, a FeCe/NC SAzyme-TMB colorimetric method for the detection of tannic acid (TA) was constructed after the optimization of catalytic conditions. The method has a high R^2 of 0.995, a low limit of detection (LOD) of 0.26 $\mu\text{mol/L}$, and high stability. The detection performance was validated by the real samples (tea). Therefore, the prepared bimetallic SAzyme FeCe/NC can be applied for TA detection without the addition of H_2O_2 , and will have broad applications in the areas of food, feed, and life science.

1. Introduction

Bio-enzymes, with highly specific catalytic capabilities, have been widely applied in various sectors, such as biomedical analysis, bio-manufacturing, and food industry production. The high cost and difficulty in long-term preservation are the challenges for their wide use, so researchers are seeking alternative catalytic materials. Since Fe_3O_4 nanoparticles with peroxidase activity were first reported in 2007, nanozymes have attracted extensive attention because of the advantages of low cost, good stability, and easy preparation (Gao et al., 2007). Henceforth, nanomaterials with enzyme-like activities, such as peroxidase, oxidase, and superoxide dismutase (SOD), have been successively developed. For example, Co_3O_4 nanoparticles with oxidase activity were used to construct a TMB- O_2 - Co_3O_4 colorimetric sensing system for the detection of sulfite (Qin et al., 2014). Wang et al. synthesized SFP@Au-CuNPs with peroxidase activity by a one-pot reduction method (Wang et al., 2023). Furthermore, regulatory strategies can be used to modulate the nanozymes' activities, e.g. the oxidase-like activity of nanoceria was cooperatively modulated with the aid of adenosine triphosphate (Cheng, Lin, Muhammad, Lin, & Wei, 2016). Up-to-date, compared with natural enzymes, nanozymes have a shortage of low catalytic activity because of the low density of active sites, which greatly hinders them in real applications. Therefore, looking for new nanozymes with higher activity is of significance.

Single-atom nanozymes (SAzymes) are one category of nanozymes. For a SAzyme, the atoms (metal) disperse in the carrier and separate from each other (Liu, 2017). Because of the high atom utilization efficiency, SAzymes have high catalytic activity (Kang et al., 2022; Xia et al., 2021). In recent years, metal-organic frameworks (MOF) materials, highly porous crystal coordination compounds composed of inorganic metal nodes and organic linkers, have been the choice for constructing SAzymes because of their large specific surface area, adjustable pore structure, and diverse components (Chen et al., 2022; Lee et al., 2023; Yu et al., 2023; Zhao et al., 2022), e.g. a multifunctional bimetallic MOF with oxygen vacancy synthesized by microplasma showed peroxidase-like, oxidase-like, and superoxide dismutase mimetic activities (Xia et al., 2024). As a kind of MOF, the zinc-based zeolite-based imidazole framework (ZIF-8) has attracted much attention because of its sodalite-like structure, abundant nitrogen-containing organic linkers, and high thermal stability (Chen et al., 2020). Chen et al. synthesized a SAzyme (Fe as the active site) by the high-temperature pyrolysis of ZIF-8, and it exhibited oxidase-like activity. Zhao et al. prepared a SAzyme (FeCo-DIA/NC with bimetallic non-alloy structure) by carbonizing FeCo-ZIF-8 precursor, it possessed both oxidase activity and peroxidase-like activity (Zhao et al., 2022). Recently, it has been reported that the single atom could be replaced by bi-atoms or multi atoms, which resulted in the increase of the SAzyme activity. For SAzyme FeN_4 , after one N was replaced with P, the SAzyme FeN_3P

* Corresponding author at: School of Biotechnology, Jiangsu University of Science and Technology, Zhenjiang 212100, China.

E-mail address: yan_hui@just.edu.cn (H. Yan).

<https://doi.org/10.1016/j.fochx.2024.101552>

Received 7 February 2024; Received in revised form 11 June 2024; Accepted 11 June 2024

Available online 19 June 2024

2590-1575/© 2024 The Author(s). Published by Elsevier Ltd. This is an open access article under the CC BY-NC license (<http://creativecommons.org/licenses/by-nc/4.0/>).

showed a higher catalytic capability (Ji et al., 2021). Wu et al. synthesized a Fe, Co, and Zn co-doped SAzyme, which showed a higher catalytic performance than that of the SAzyme containing a single metal element (Wu et al., 2022). Therefore, the construction of a SAzyme with bimetal or multimetal elements is an effective strategy to enhance the catalytic activity of SAzymes.

Ce is one of the most abundant elements on earth and its price is low compared with other rare earth metals (Shan, Liu, Li, & Yang, 2020; Yang, Wang, Song, & Zhang, 2019). In addition, because of its special outer electron structure $[Xe]4f^15d^16s^2$, Ce has a significant redox pair (Ce^{3+}/Ce^{4+}) (Shan et al., 2020; Yang et al., 2019). The nanozymes composed of Ce have been investigated, for example, CeO_2 has peroxidase-like activity (Pirmohamed et al., 2010); Hang et al. synthesized three typical nanostructures of nanorods, nanopolyhedra, and nanocubes by adjusting the scale of nanozymes, and found that they had oxidase-like activity (Huang et al., 2017). However, most of these studies focused on CeO_2 , and reports showed that with the particle size decreased their surface free energy was greatly increased, which further improved their catalytic activity (Li et al., 2021; Yang et al., 2013). Hence, the development of the nanozymes containing Ce was very promising.

Tannic acid (TA) is a category of important ingredients in tea. On the one hand, TA is a polyphenol acid possessing antioxidant, anticarcinogenic, anti-mutagenic, and anti-inflammatory properties (Moulick et al., 2023). On the other hand, it has negative health impacts such as nausea and stomach irritation if consumed in large quantities (Rodríguez, de Las Rivas, Gómez-Cordovés, & Muñoz, 2008). Therefore, the detection of TA content in tea is very important.

Herein, we designed and constructed a new bimetal SAzyme FeCe/NC, which had higher oxidase-like activity, compared with the traditional single metal SAzyme Fe/NC. The process of preparation and application is shown in Scheme 1. Firstly, the FeCe-ZIF-8 was prepared, and then the bimetal SAzyme FeCe/NC was obtained by high-temperature pyrolysis. It has oxidase-like activity, and could catalytic oxidase O_2 to generate reactive oxygen species (ROS) of $\bullet OH$, $O_2^{\bullet -}$ and

1O_2 , which could catalyze the oxidation of TMB to blue oxTMB. Then, a FeCe/NC SAzyme -TMB colorimetric method for the quantitative detection of TA was constructed.

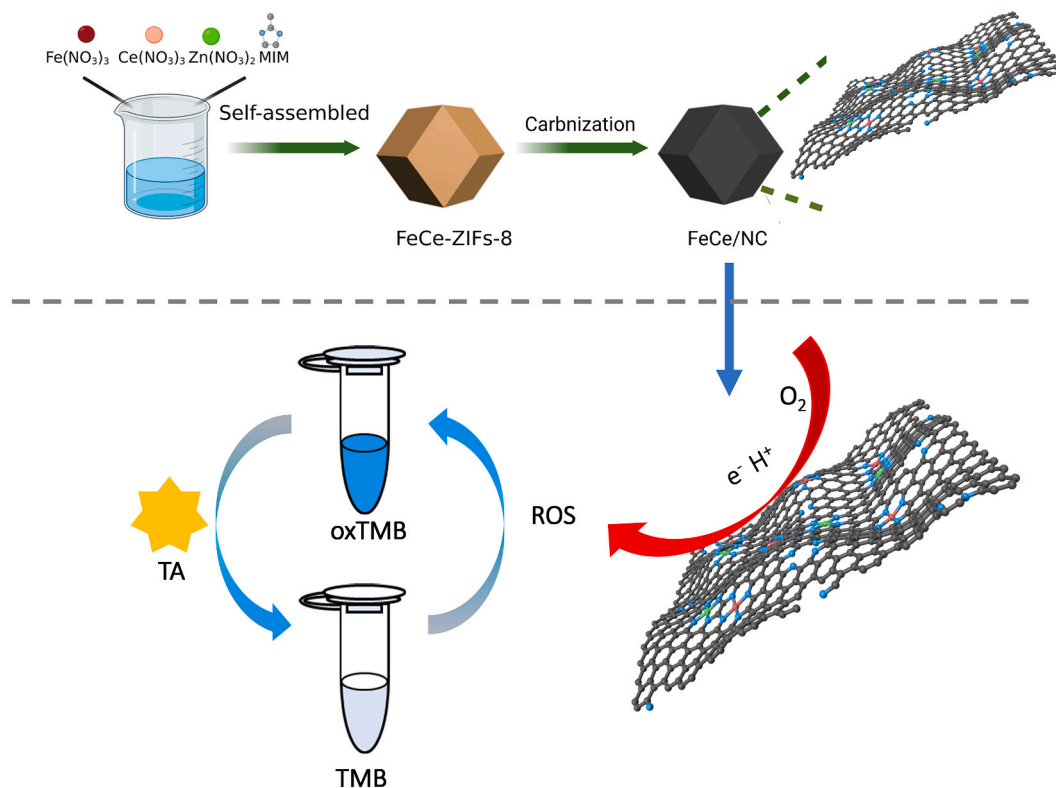
2. Materials and methods

2.1. Materials

Zinc nitrate ($Zn(NO_3)_2 \cdot 6H_2O$), iron nitrate ($Fe(NO_3)_3 \cdot 9H_2O$), 2-methylimidazole (MIM), 3,3',5,5'-tetramethylbenzidine (TMB), *o*-phenylenediamine (OPD), Zinc standard (1000 $\mu g/mL$), and 2,2'-azino-bis(3-ethylbenzothiazoline-6-sulfonic acid) diammonium salt (ABTS) were purchased from Shanghai Aladdin Biochemical Technology Co., Ltd. (Shanghai, China). Cerium nitrate ($Ce(NO_3)_3 \cdot 6H_2O$) was supported by Shanghai Yien Chemical Technology Co., Ltd. (Shanghai, China). Methanol, acetic acid (HAc), ascorbic acid (AA), and sodium acetate (NaAc) were purchased from Shanghai Sinopharm Chemical Reagent Company (Shanghai, China). All chemicals were of analytical reagent grade.

2.2. Instruments

The morphology of the SAzyme was characterized by High-resolution transmission electron microscopy (HRTEM) (TF-G20, Thermo Fisher Scientific, Waltham, MA, USA), scanning electron microscopy (SEM) (Regulus-8100, Hitachi, Tokyo, Japan), and X-ray diffractometer (XRD) (D8-Advance, Bruker, Saarbrücken, Saarland, Germany). X-ray photoelectron spectroscopy (XPS) (AXIS ULTRA DLD, Shimadzu, Tokyo, Japan) was used to investigate the surface composition and bonding state of the nanocrystals. Electron spin resonance (ESR) was characterized by a paramagnetic resonance spectrometer (A300, Bruker, Saarbrücken, Saarland, Germany). BET Specific surface area was characterized using a specific surface area & pore size analyzer (JW-DK200B, Precision & Microtech, Beijing, China) for characterization. The concentrations of zinc in the materials were determined using



Scheme 1. Principle of the FeCe/NC SAzymes-TMB colorimetric sensor for TA detection.

an inductively coupled plasma mass spectrometry (ICP-MS, X Series II, Thermo Scientific).

2.3. Methods

2.3.1. Synthesis of FeCe/NC

The particle size of ZIF-8 is affected by the ratio of methanol to Zn^{2+} , the larger the ratio, the smaller the particle size. The activity of SAzymes has a relationship with their particle size, the smaller the particle size, the higher the activity. However, too small a particle size will lead to the aggregation of SAzymes, resulting in the decrease of SAzyme activity. Therefore, the appropriate particle size is crucial for SAzyme activity.

SAzyme FeCe/NC was synthesized according to the literature (Zhang et al., 2017), wherein the optimal molar ratio among $Fe(NO_3)_3 \cdot 9H_2O$, $Zn(NO_3)_2 \cdot 6H_2O$, and MIM and amounts of methanol based on its molar ratio to Zn^{2+} were applied in this work. In order to prepare the bimetallic SAzyme FeCe/NC, $Ce(NO_3)_3 \cdot 6H_2O$ was added to the above solution (Zhao et al., 2022). Through the investigation of the amount of $Ce(NO_3)_3 \cdot 6H_2O$ (Fig. S1, shown in Supplementary data), the optimal preparation method was obtained. Briefly, solution A (0.1 g $Fe(NO_3)_3 \cdot 9H_2O$, 2.975 g $Zn(NO_3)_2 \cdot 6H_2O$, 3.126 g $Ce(NO_3)_3 \cdot 6H_2O$, and 265 mL of methanol) and solution B (3.456 g MIM and 265 mL of methanol) were prepared, respectively. Solution A was added to solution B and stirred vigorously for 2 h, left to age for 24 h. The yellow precipitate was collected and washed several times with methanol, and dried at 60 °C to yield precursor FeCe-Zn ZIFs, then it was loaded in a quartz boat and heated at a rising rate of 5 °C/min in an N_2 atmosphere. Additionally, in order to investigate the influence of temperature on the SAzyme activity, the pyrolysis temperatures of 600, 700, 800, 900, 1000, and 1100 °C were maintained for 2 h, respectively. In order to compare the catalytic properties of SAzyme FeCe/NC, SAzyme Fe/NC was synthesized using the same method, in which $Ce(NO_3)_3 \cdot 6H_2O$ was not added (Zhang et al., 2017). The concentrations of zinc in the ZIF-8 and FeCe@ZIF-8 were determined by ICP-MS with collision cell technology, for which helium and hydrogen (7%) mixture as reaction collision gas. Before the ICP-MS analysis, the samples were digested with boiled aqua regia.

2.3.2. Investigation of the catalytic mechanism of SAzyme FeCe/NC

Two 500 µg/mL SAzyme FeCe/NC dispersions were bubbled with N_2 and O_2 for 30 min to obtain the N_2 or O_2 saturated solutions, respectively. The same processing was conducted for 200 mmol/L acetate buffer (pH 3.5). Subsequently, 0.1 mL 500 µg/mL SAzyme FeCe/NC and 0.1 mL 4 mmol/L TMB were added to 1.8 mL 200 mmol/L acetate buffer and incubated at 30 °C for 12 min under the corresponding N_2 or O_2 protection. Then the absorbance at 652 nm was measured by a UV-Vis spectrometer.

To interpret the mechanism of SAzyme FeCe/NC catalytic oxidation of TMB, ESR was used to detect the generated 3 kinds of ROS $\bullet OH$, $O_2^{\bullet -}$, and 1O_2 , respectively. The spin trapping agent 5,5-dimethyl-1-pyrroline N-oxide (DMPO) was used to capture $\bullet OH$ in water and to capture $O_2^{\bullet -}$ in methanol, respectively, and the trapping agent 2,2,6,6-Tetramethyl-4-piperidone hydrochloride (TEMP) was used to capture 1O_2 in water.

2.3.3. Oxidase-like activity

In order to assess the oxidase-like activity, TMB was selected as the colorimetric substrate. SAzyme FeCe/NC catalyzed colorless TMB to generate blue oxTMB, which had an absorption peak at 652 nm. 100 µL 500 µg/mL SAzyme FeCe/NC was added to 1.8 mL 200 mmol/L acetate buffer (pH 3.5), followed by the addition of 100 µL 4 mmol/L TMB. Then the mixture was incubated at 30 °C and the absorbance was measured. To investigate the influence of pH on the SAzyme activity, the reactions were performed at different pH (2, 3, 3.5, 4.5, and 6). Likewise, the effects of temperature and SAzyme concentration on the catalytic activity were investigated.

2.3.4. Steady-state kinetics of FeCe/NC SAzyme

Firstly, 0.1 mL of 500 µg/mL SAzyme FeCe/NC was added to 1.8 mL of 200 mmol/L acetic acid buffer (pH 3.5). Then 0.1 mL of different concentrations (0.01, 0.02, 0.03, 0.05, 0.1, 0.2, 0.3, 0.5, 0.8, and 1 mmol/L) of TMB were added, respectively. Recorded the absorbance at 30 °C every 1 min after 30 s of reaction. The concentration of oxTMB was calculated based on Beer-Lambert law ($A = kbC$), where A is the absorbance at 652 nm, k is the molar absorptivity of oxTMB of 39,000 $M^{-1} cm^{-1}$, b is the optical path in cm, and C is the concentration of the substrate. Finally, the kinetic parameters were obtained by fitting Lineweaver-Burk equation.

2.3.5. Establishment of the colorimetric method for the detection of TA

Added 0.1 mL of 4 mg/L SAzyme FeCe/NC to 1.7 mL of 200 mmol/L acetic acid buffer (pH 3.5), and then added 0.1 mL TA (1.0–6.0 µmol/L), finally, 0.1 mL 4 mmol/L TMB was added at 30 °C for 12 min, then recorded the absorbance. The control was without TA. The inhibition rate was calculated based on the absorbance difference ΔA ($\Delta A = A_{control} - A_{TA}$). The linear range, limit of detection (LOD), repeatability, and reproductivity were investigated.

To evaluate the selectivity of the FeCe/NC SAzyme-TMB sensing system, some ions and amino acids including Na^+ , K^+ , Ca^{2+} , Arginine (Arg), Glycine (Gly), Glutamic acid (Glu), and Methionine (Met) were applied.

2.3.6. Detection of real samples

In order to validate the detection performance of the method, three kinds of tea purchased from the local supermarket were applied. 1.6 g of each tea was soaked in 60 mL boiling water for 5 min, subsequently, the tea soup liquid cooled down to room temperature and passed through a 0.22 µmol/L membrane. After appropriate dilution, it was detected with the established method. The detection results were compared with the standard method Folin phenol.

3. Results and discussion

3.1. Synthesis of SAzyme FeCe/NC

In the preparation of SAzyme FeCe/NC, Fe in Fe and Ce were wrapped in ZIF-8 to form bimetallic doped FeCe@ZIF-8.

As shown in Fig. S2, the pattern of XRD of the FeCe@ZIF-8 was the same as that of ZIF-8, which demonstrated that FeCe@ZIF-8 was a ZIF-8-like structure. Based on Scherer equation, the size of the ZIF-8 and FeCe@ZIF-8 were calculated, they were 81 nm and 129 nm, respectively. Interestingly, the size of FeCe@ZIF-8 was enlarged after Ce and Fe were introduced. This change needed to be further studied and understood, which has a guiding significance for the preparation of highly active SAzymes in the future.

The oxidase-like activity of SAzyme FeCe/NC is mainly related to its specific surface area, active site density, and electronic conductivity, which can be regulated by changing the pyrolysis temperature. As shown in Fig. S3, the SAzyme activity increased with the rise of temperature within 600–1000 °C, and reached the highest activity at 1000 °C, then it descended with the further rise of temperature. Therefore, 1000 °C was the optimal pyrolysis temperature.

3.2. Characterization of the prepared FeCe/NC SAzyme

3.2.1. Transmission electron microscopy

As shown in Fig. 1a, the TEM revealed that SAzyme FeCe/NC appeared regular dodecahedral structure of ZIF-8 with an average diameter of 120 nm, and Fig. 1b showed that it had a porous carbon structure with abundant well-like edges, they could be used to store active sites, which was beneficial for the catalytic reaction. The element mapping (Fig. 1c) showed that each kind of element was uniformly distributed in SAzyme FeCe/NC.

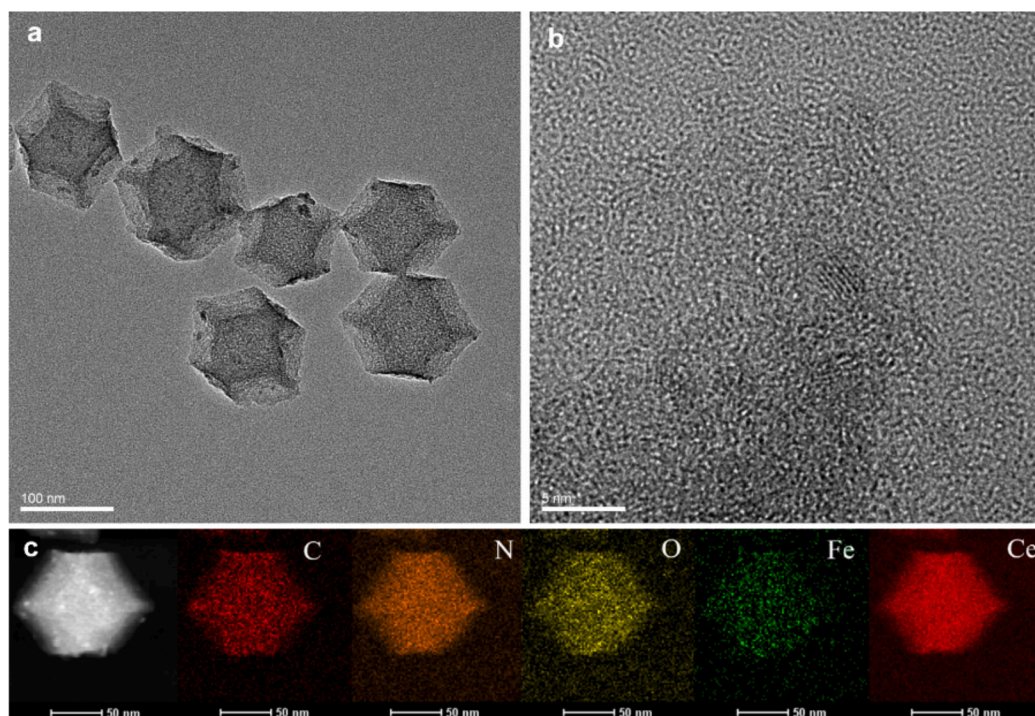


Fig. 1. Characterization of the prepared SAzyme FeCe/NC, HRTEM image of FeCe/NC with low magnification (a) and high magnification (b), element mapping of C, N, O, Fe, and Ce (c).

3.2.2. XRD and specific surface area

XRD patterns of FeCe/NC SAzyme and N—C are shown in Fig. S4A, they have two diffraction peaks at about 25° and 43° , which belong to carbon (002) and carbon (101), respectively. In addition, no other characteristic peaks appeared, demonstrating that there were no crystal forms of metals, metal oxides, and metal carbides during the pyrolysis process (Zhao et al., 2022). Furthermore, to investigate the specific surface area of SAzyme FeCe/NC, N_2 adsorption–desorption isotherms were performed. As shown in Fig. S4B, the BET specific surface area was $487.5 \text{ m}^2/\text{g}$, which was similar to that of other reported Fe/NC (Chen, Liang, Zhang, & Huang, 2018), it was crucial for the catalytic activity.

3.2.3. XPS analysis

To investigate the chemical composition and state of SAzyme FeCe/NC, XPS measurements were performed. As shown in Fig. 2A, SAzyme FeCe/NC was composed of C, N, O, Fe, and Ce, which was consistent with the elemental mapping analysis results. There was no characteristic peak of Zn 2p around 1020 eV, which demonstrated that there was no Zn existing in the material. Furthermore, the contents of Zn in Fe/NC and FeCe/NC were measured by ICP-MS, and they were nearly zero (0.010% and 0.012%). It was because that, at temperatures above 800°C , Zn was reduced to its zero valence state, and was evaporated at the pyrolysis temperature 1000°C (used in this work), which was higher than the boiling point (907°C) of Zn.

In Fig. 2B, the peak fitting for N 1s XPS spectrum showed four main peaks at 398.2 eV, 399.3 eV, 400.8 eV, and 405.0 eV, indicating the coexistence of four types of N, which were pyridinic N, pyrrole N, graphitic N, and oxidized N (Song et al., 2022). Due to the electron-donating properties of pyridines and pyrroles, properly arranged pyridinic Ns could serve as anchor sites for Fe and Ce; meanwhile, free pyridinic Ns could also capture protons and O_2 , and then transfer them to the active center (Zhao, Watanabe, & Hashimoto, 2012). Therefore, it speculated that the content of pyridine N directly affected the catalytic activity of the SAzyme, and the higher the proportion of pyridine N, the higher the catalytic activity. In addition, according to the relevant literature (Zhang et al., 2017), graphite N could not only affect the

structure of carbon, but also improve electrical conductivity accelerate electron transfer, and ultimately improve the catalytic activity of the SAzyme. As shown in Fig. 2C, the peak fitting for Fe 2p XPS spectrum showed four main peaks at 710.6 eV (Fe^{2+}), 720.4 eV (Fe^{2+}), 712.9 eV (Fe^{3+}) and 723.0 eV (Fe^{3+}), and the other peaks at 716.1 eV ($Fe^{2+} 2p_{3/2}$), 718.5 eV ($Fe^{3+} 2p_{3/2}$), 728.2 eV ($Fe^{2+} 2p_{1/2}$), and 731.89 eV ($Fe^{3+} 2p_{1/2}$). This redox-induced transition between Fe^{2+} and Fe^{3+} might play an important role in the catalytic reaction (Jung, Lim, Park, & Kim, 2009). As shown in Fig. 2D, the peak fitting for Ce 3d XPS spectrum showed eight main peaks of m_1 (883.0 eV), m_2 (886.5 eV), m_3 (890.0 eV), m_4 (898.6 eV), n_1 (901.2 eV), n_2 (903.7 eV), n_3 (907.6 eV) and n_4 (917.8 eV), among which m_2 and n_2 belong to Ce^{3+} , and the other six belong to Ce^{4+} . This redox-induced transition between Ce^{3+} and Ce^{4+} might play an important role in the catalytic reaction (Li et al., 2021).

3.3. Catalytic mechanism of SAzyme FeCe/NC

The enzyme catalytic activities of SAzyme FeCe/NC in saturated O_2 , air, and N_2 solutions were compared. As shown in Fig. 3A, there were obvious differences in the absorbance peak at 652 nm when TMB was catalyzed. For O_2 , air, and N_2 , the absorbance was 1.95, 1.24, and 0.253, which demonstrated that the catalytic oxidation of TMB by SAzyme FeCe/NC was O_2 dependent. To investigate the specific ROS generation process in the catalytic reaction, ESR technology was used. As shown in Fig. 3B, when DMPO was used as the $\bullet OH$ scavenger in water, the ESR characteristic peak was shown as 1:2:2:1, which was the typical peak pattern of $\bullet OH$ (Chen et al., 2020), therefore, SAzymeFeCe/NC catalyzed O_2 to generate $\bullet OH$. Similarly, as shown in Fig. 3C, when DMPO was used as the $O_2^{\bullet -}$ capture agent in methanol, the ESR characteristic peaks were shown as 1:1:1:1, which was the unique peak shape of $O_2^{\bullet -}$, demonstrating that SAzyme FeCe/NC catalyzed O_2 to generate $O_2^{\bullet -}$ (Wu et al., 2019). When TEMP was used as the 1O_2 capture agent in water, the ESR characteristic peak pattern was 1:1:1 (Fig. 3D), belonging to 1O_2 , it demonstrated that SAzyme FeCe/NC produced 1O_2 during the catalytic process (Zhao et al., 2022). Therefore, it demonstrated that SAzyme FeCe/NC could catalyze O_2 to produce the ROS of $\bullet OH$, $O_2^{\bullet -}$, and

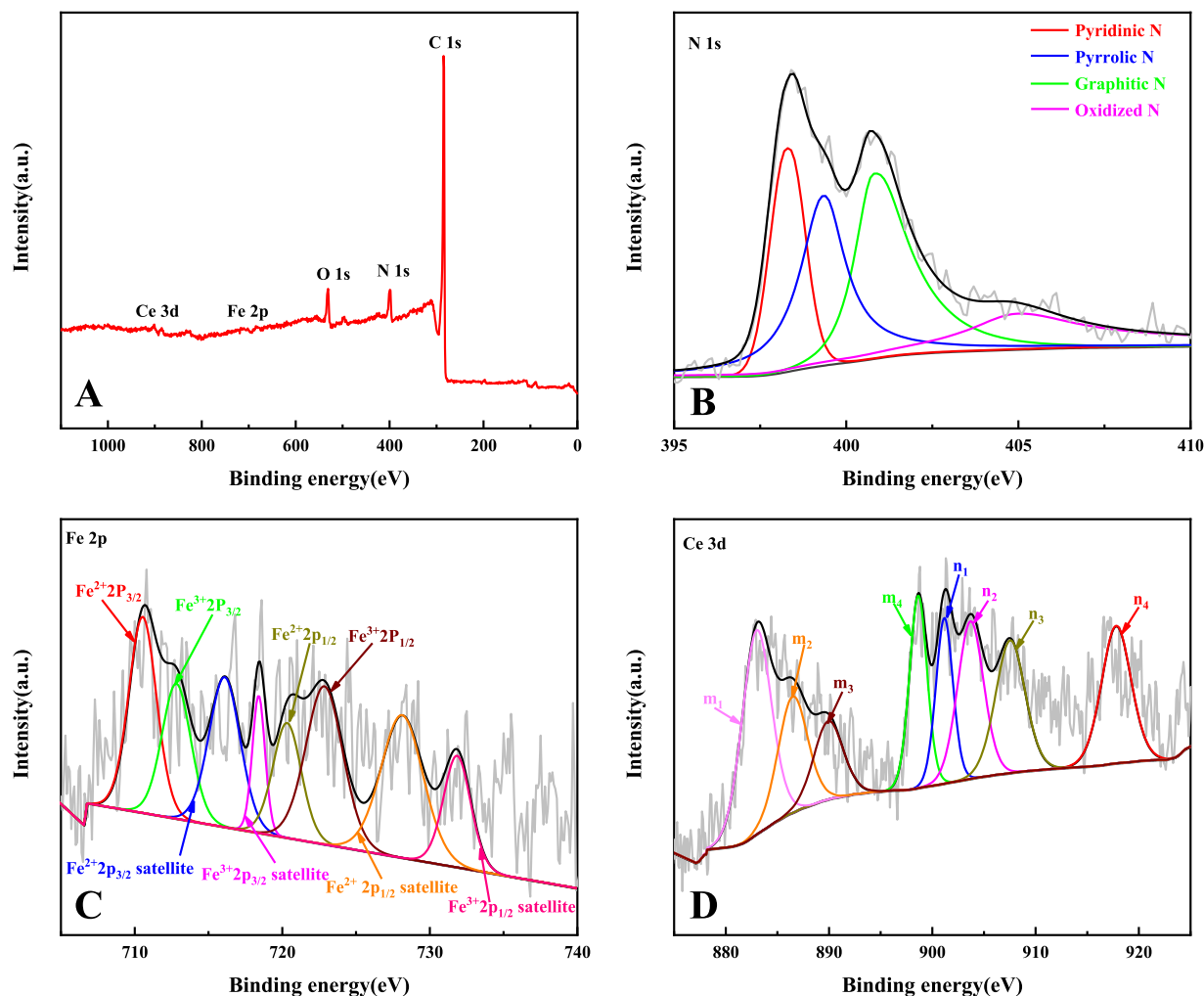
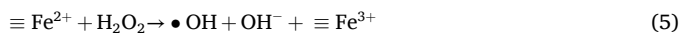
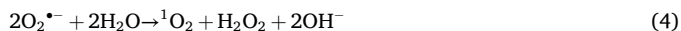
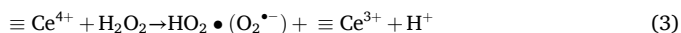
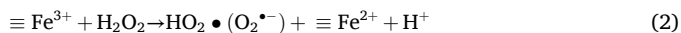


Fig. 2. XPS spectrum of SAzyme FeCe/NC and its interpretation, XPS spectrum of FeCe/NC SAzymes (A); XPS spectral analysis for N 1 s (B), Fe 2p (C) and Ce 3d (D).

$O_2^{\bullet -}$.

Based on the above results, the catalytic mechanism was obtained. Firstly, O_2 was adsorbed onto the surface of SAzyme FeCe/NC to obtain $2e^-$ from TMB and $2H^+$ in an acidic medium, and it was itself oxidized and reduced to generate H_2O_2 (Chen et al., 2020; Li et al., 2021), which was then adsorbed onto SAzyme FeCe/NC to reduce Fe^{3+} and Ce^{4+} in SAzyme FeCe/NC to generate $HO_2\bullet(O_2^{\bullet -})$ (Li et al., 2021). $O_2^{\bullet -}$ was disproportionated into 1O_2 and H_2O_2 , and H_2O_2 reacted with Fe^{2+} and Ce^{3+} to generate $\bullet OH$ through Fenton-like reactions. The generated Fe^{3+} and Ce^{4+} returned and started a new cycle to achieve the ROS loop (Chen et al., 2021; Wang et al., 2019). The ROS (1O_2 , $O_2^{\bullet -}$, and $\bullet OH$) oxidized TMB to generate oxTMB. Based on this principle, an analytical method can be constructed, and it is convenient for users since without the addition of H_2O_2 , compared to similar methods that rely on catalase.



3.4. Substrates selection for SAzyme FeCe/NC

To systemically assess the oxidase-like activity of SAzyme FeCe/NC, 3 chromogenic substrates of TMB, ABTS, and OPD were employed. As shown in Fig. S5A, blue oxTMB presented an obvious absorption peak at 652 nm, green oxABTS appeared an absorption peak at 412 nm, and yellow oxOPD had an absorption peak at 450 nm. Compared with the other two substrates, TMB is non-carcinogenic and is oxidized quickly, therefore, it was chosen as the substrate for future applications. As shown in Fig. S5B, TMB, SAzyme FeCe/NC, and TMB + SAzyme FeCe/NC were added to the acetic acid buffer (200 mmol/L, pH 3.5), respectively, and only the solution containing both TMB and SAzyme FeCe/NC turned blue. It demonstrated that the color change of TMB was caused by the oxidase-like activity of SAzyme FeCe/NC.

3.5. Steady-state kinetic analysis of SAzyme FeCe/NC

The results of the Steady-state Kinetic Analysis of SAzyme FeCe/NC and Fe/NC are presented in Fig. S6A and Fig. S6C, which exhibited a typical Michaelis-Menten curve. The maximum reaction rate (V_{max}) and the Michaelis constant (K_m) were obtained by the fitting with Lineweaver-Burk equation (eq. 8).

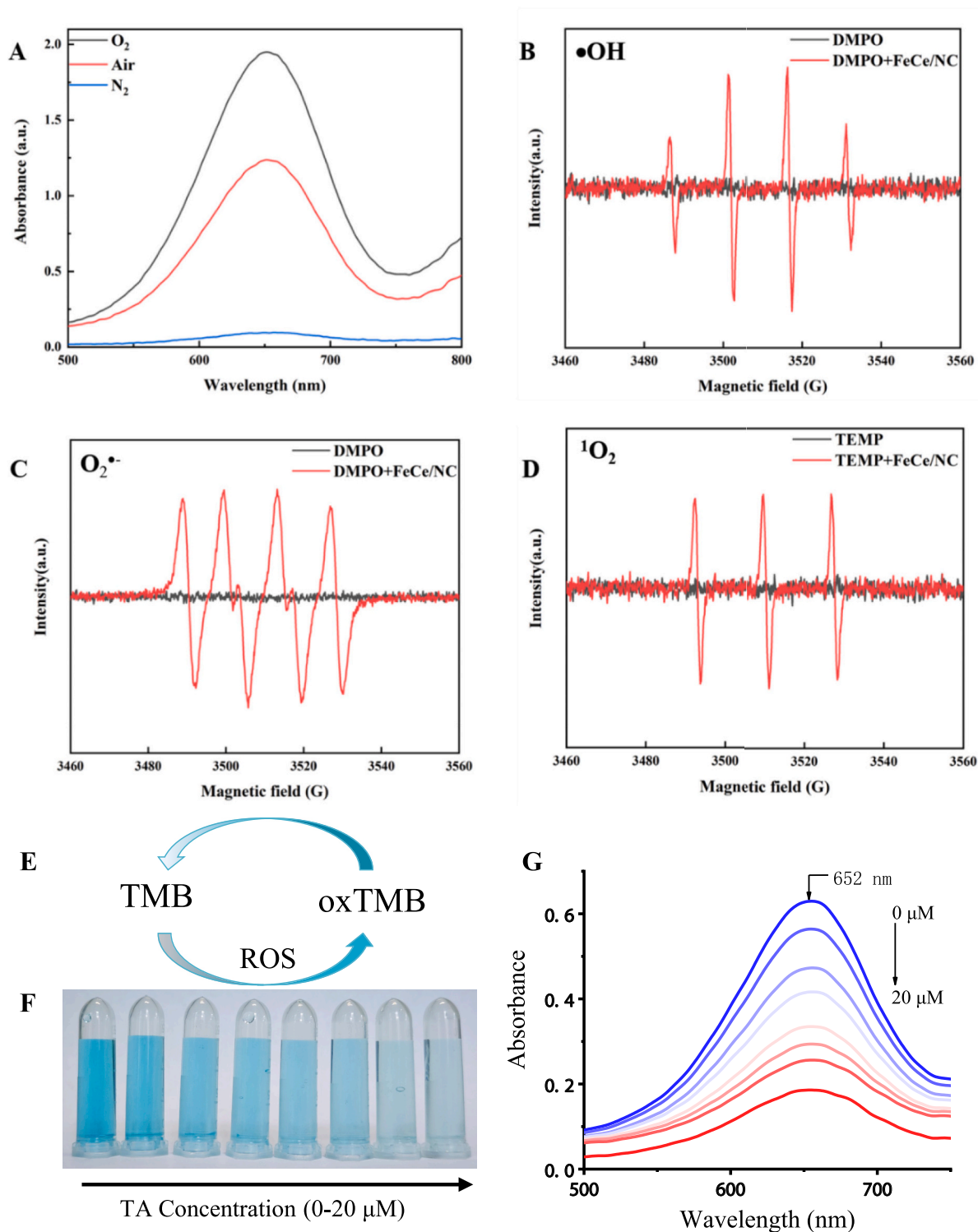


Fig. 3. Investigation of the mechanism of FeCe/NC SAzyme-TMB colorimetric method for TA detection, UV-vis spectra of FeCe/NC SAzyme-TMB sensing system in O₂, air, and N₂ saturated solutions (A), ESR spectrum for the detection of •OH, O₂^{•-}, and ¹O₂ (B–D), the effect of ROS and TA on TMB and oxTMB, respectively (E), the color of the FeCe/NC TMB solution with different concentrations of TA (F), and the visible spectra of the FeCe/NC TMB solution with different concentrations of TA (G).

$$\frac{1}{V_0} = \frac{K_m}{V_{max}} \cdot \frac{1}{[S]} + \frac{1}{V_{max}} \quad (8)$$

The fitted equations of SAzyme FeCe/NC and SAzyme Fe/NC were $y = 0.019x + 0.146$ (Fig. S6B), $R^2 = 0.998$ and $y = 0.042x + 0.179$ (Fig. S6D), $R^2 = 0.993$, respectively. The V_{max} and K_m of SAzyme FeCe/NC were $7.68 \times 10^{-7} \text{ M s}^{-1}$ and 0.15 mmol/L , respectively, and the V_{max} and K_m of SAzyme Fe/NC were $5.59 \times 10^{-7} \text{ M s}^{-1}$ and 0.237 mmol/L ,

respectively. Generally, the lower the K_m value, the stronger the interaction between an enzyme and its substrate. In this work, the K_m value of SAzyme FeCe/NC was lower than that of SAzyme Fe/NC, which demonstrated that SAzyme FeCe/NC had a higher catalytic performance.

Compared with SAzyme Fe/NC, the oxidase-like activity of SAzyme FeCe/NC was enhanced, which could be attributed to the following

reasons: (1) the synergistic effect of Fe and Ce bimetallic active centers (Zhao et al., 2022), (2) SAzyme FeCe/NC has a high BET specific surface area, which exposed more active sites and increased the contact probability between O₂ and SAzyme FeCe/NC (Chen et al., 2021).

3.6. Optimization of the colorimetric sensing system

The catalytic activity of SAzyme FeCe/NC, like that of natural enzymes, was influenced by the reaction conditions. Therefore, the effects of pH, reaction time, reaction temperature, and catalyst concentration on the catalytic performance of SAzyme FeCe/NC were investigated.

Firstly, pH was optimized, as shown in Fig. S7A, and SAzyme FeCe/NC presented the highest activity at pH 3.5. The reason was that, on the one hand, under pH 2 and 3, it agglomerated in the solution, resulting in the reduction of catalytic active sites, which decreased its catalytic activity. Furthermore, when pH was 2, free residual chlorine reacted with TMB to form a yellow quinoid compound, which had no absorbance at 652 nm. On the other hand, the solubility of TMB was very low under alkaline conditions, which led to low substrate concentration, accordingly, the product was less. Therefore, the optimal pH was 3.5.

Next, the reaction time was investigated. As shown in Fig. S7B, it tended to equilibrium at 12 min, which was selected as the optimal reaction time.

As shown in Fig. S7C, in the range of 20–30 °C, with the temperature increase, the oxidase-like activity rose, however, it gradually decreased with the further increase of temperature. Therefore, 30 °C was the optimal temperature.

Fig. S7D is the effect of SAzyme FeCe/NC concentration on the catalytic activity. In the range of 0–25 mg/L, the oxidase-like activity rose with the increase of the catalyst concentration, however, it tended to be stable when the concentration was higher than 25 mg/L. Therefore, 25 mg/L was the optimal concentration of SAzyme FeCe/NC.

3.7. Colorimetric method for the detection of TA

The SAzyme FeCe/NC generated ROS to oxidize colorless TMB to produce blue oxTMB, and TA could reduce oxTMB to TMB (Wang et al., 2024; Xie et al., 2023), therefore, a novel colorimetric strategy was constructed to detect TA (Fig. 3E). To assess the feasibility of the SAzyme-TMB system for TA detection, preliminary experiments were performed. As shown in Fig. 3F, in the absence of TA, the system appeared blue (the 1st left centrifuge tube), and a large absorbance at 652 nm was presented on its corresponding absorption spectrum (Fig. 3G). When a low concentration (1 μM) of TA existed in the system, it had a minor influence on the response of the system, and blue slightly weakened (the 2nd left centrifuge tube shown in Fig. 3F). However, with the concentration of TA increased (3, 5, 8, 10, 15, 20 μM), blue continuously weakened (inset in Fig. 3F). It was because more TA reduced more oxTMB to TMB, and it was clear that obvious color changes could be observed and the A₆₅₂ declined gradually with TA increase (inset in Fig. 3G). So, a colorimetric strategy could be developed to detect TA content. Subsequently, the parameters of the detection system were optimized.

3.7.1. Optimization of SAzyme FeCe/NC concentration in the sensing system

To improve the detection performance of the biosensor, the concentration of SAzyme FeCe/NC was investigated. As shown in Fig. S8, the optimal concentration of 4 mg/L was easily obtained.

3.7.2. Establishment of working curve

Under the optimal conditions (pH 3.5 and temperature 30 °C), the absorbance (652 nm) under different concentrations of TA was measured at 12 min of reaction. As shown in Fig. 4, the concentration of TA in the range of 1.0–6.0 μmol/L had a linear relationship with the absorbance, and the regression equation was $y = 0.0446x + 0.0394$,

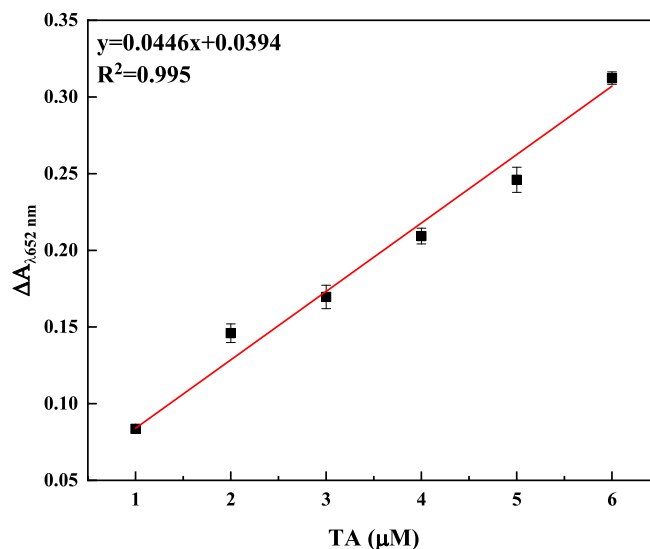


Fig. 4. Linear regression curve between TA concentration and $\Delta A_{652 \text{ nm}}$ of the FeCe/NC SAzyme-TMB sensing system for TA detection.

where y and x were the decrease of absorbance and the concentration of TA, respectively, the coefficient of determination R^2 was 0.995, demonstrating that they existed a good linear relationship. The LOD was 0.26 μmol/L by the calculation (Signal/Noise = 3), demonstrating that the FeCe/NC SAzyme-TMB colorimetric sensor was sensitive to TA.

3.7.3. Selectivity of TA detection

To investigate the anti-interference capability of the constructed method, the interfering substances of Ca²⁺, K⁺, Na⁺, Arg, Gly, Glu, and Met were added to the sensing system. Here, each of the interfering substances was 100 μmol/L, much higher than the maximum detection concentration of TA. As shown in Fig. S9, for the samples containing interfering substances, the absorbance remained almost unchanged, like that of the blank. Only the TA-added sample presented a significant decrease in absorbance, which demonstrated that the established biosensor had high selectivity.

3.7.4. Repeatability and reproducibility of FeCe/NC SAzymes-TMB colorimetric sensor

For the evaluation of the repeatability of the constructed biosensor, three parallel tests were conducted on the sample containing 5.0 μmol/L TA, and the results showed that the relative standard deviation (RSD) was 3.22%, demonstrating that the sensing system has good repeatability. After the synthesized SAzyme FeCe/NC was stored at room temperature for 30 days, it was used to detect the 5 μmol/L TA sample, the test result was 4.54 ± 0.09 μmol/L. The absolute error was 0.46 μmol/L, and the RSD was 1.67% (<5%), therefore, the method has good reproducibility for the TA detection.

3.7.5. Validation of the method with real sample tea

To validate the detection performance of the constructed sensor, sample tea was tested. Folin phenol method was applied as the reference method (Piovesan, Santana, & Spinelli, 2020). The results are presented in Table 1. The absolute errors and relative errors were low, which were acceptable. The RSDs of the method were 5.97%, 3.78%, and 2.35%, respectively, which demonstrated that it had high stability. There was no statistical difference between the results of this method and those of the reference method ($P > 0.05$), which demonstrated that the performance of the method was as same as that of the reference method. Therefore, the established method could accurately detect TA in tea.

Table 1

Results comparison of the method between Folin phenol and the developed for the detection of TA in tea.

Tea No.	Folin method (g kg ⁻¹)	This method (g kg ⁻¹)	Absolute error (g kg ⁻¹)	Relative error (%)	RSD (%)	P
1	21.43 ± 0.32	19.67 ± 1.17	-1.76	8.21	5.97	0.11
2	37.52 ± 0.14	38.89 ± 1.47	1.37	3.65	3.78	0.25
3	53.22 ± 1.18	54.15 ± 1.27	0.93	1.75	2.35	0.41

4. Conclusions

The bimetallic SAzyme FeCe/NC with high oxidase-like activity was successfully constructed, and its catalytic mechanism was that it activated O₂ to generate the ROS of •OH, O₂^{•-} and ¹O₂. On these grounds, a FeCe/NC SAzyme - TMB colorimetric biosensor was constructed for TA detection with high detection performance. In addition, it is convenient for users since without the addition of H₂O₂. Therefore, the construction of a bimetallic SAzyme is a feasible strategy to obtain a higher activity SAzyme, with the advantages of low-cost, easy, and long-term storage, it will be beneficial to substitute natural enzymes in the application of food, feed, and life science, and will have broad application prospects.

Fundings

This work was supported by the earmarked fund for CARS-18, and Graduate Research and Innovation Projects of Jiangsu Province (grant number KYCX23_3841).

CRedit authorship contribution statement

Xingyu Zhu: Writing – original draft, Methodology, Investigation. **Chong Chen:** Methodology, Investigation. **Dou Che:** Investigation. **Hui Yan:** Writing – review & editing, Supervision, Resources, Methodology, Funding acquisition, Conceptualization.

Declaration of competing interest

The authors declare that they have no known competing financial interests or personal relationships that could have appeared to influence the work reported in this paper.

Data availability

Data will be made available on request.

Appendix A. Supplementary data

Supplementary data to this article can be found online at <https://doi.org/10.1016/j.fochx.2024.101552>.

References

- Chen, J., Zheng, X., Zhang, J., Ma, Q., Zhao, Z., Huang, L., Wu, W., Wang, Y., Wang, J., & Dong, S. (2021). Bubble-templated synthesis of nanocatalyst co/C as NADH oxidase mimic. *National Science Review*, 9(3), Article nwab186. <https://doi.org/10.1093/nsr/nwab186>
- Chen, Q., Li, S., Liu, Y., Zhang, X., Tang, Y., Chai, H., & Huang, Y. (2020). Size-controllable Fe-N/C single-atom nanozyme with exceptional oxidase-like activity for sensitive detection of alkaline phosphatase. *Sensors and Actuators B: Chemical*, 305, Article 127511. <https://doi.org/10.1016/j.snb.2019.127511>
- Chen, Q., Liang, C., Zhang, X., & Huang, Y. (2018). High oxidase-mimic activity of Fe nanoparticles embedded in an N-rich porous carbon and their application for sensing of dopamine. *Talanta*, 182, 476–483. <https://doi.org/10.1016/j.talanta.2018.02.032>
- Chen, Q., Liu, Y., Lu, Y., Hou, Y., Zhang, X., Shi, W., & Huang, Y. (2022). Atomically dispersed Fe/bi dual active sites single-atom nanozymes for cascade catalysis and

- peroxymonosulfate activation to degrade dyes. *Journal of Hazardous Materials*, 422, Article 126929. <https://doi.org/10.1016/j.jhazmat.2021.126929>
- Cheng, H., Lin, S., Muhammad, F., Lin, Y.-W., & Wei, H. (2016). Rationally modulate the oxidase-like activity of nanoceria for self-regulated bioassays. *ACS Sensors*, 1(11), 1336–1343. <https://doi.org/10.1021/acssensors.6b00500>
- Gao, L., Zhuang, J., Nie, L., Zhang, J., Zhang, Y., Gu, N., Wang, T., Feng, J., Yang, D., & Perrett, S. (2007). Intrinsic peroxidase-like activity of ferromagnetic nanoparticles. *Nature Nanotechnology*, 2(9), 577–583. <https://doi.org/10.1038/nnano.2007.260>
- Huang, L. J., Zhang, W. T., Chen, K., Zhu, W. X., Liu, X. N., Wang, R., ... Wang, J. L. (2017). Facet-selective response of trigger molecule to CeO {110} for up-regulating oxidase-like activity. *Chemical Engineering Journal*, 330, 746–752. <https://doi.org/10.1016/j.cej.2017.08.026>
- Ji, S., Jiang, B., Hao, H., Chen, Y., Dong, J., Mao, Y., Zhang, Z., Gao, R., Chen, W., & Zhang, R. (2021). Matching the kinetics of natural enzymes with a single-atom iron nanozyme. *Nature Catalysis*, 4(5), 407–417. <https://doi.org/10.1038/s41929-021-00609-x>
- Jung, Y. S., Lim, W. T., Park, J. Y., & Kim, Y. H. (2009). Effect of pH on Fenton and Fenton-like oxidation. *Environmental Technology*, 30(2), 183–190. <https://doi.org/10.1080/09593330802468848>
- Kang, G., Liu, W., Liu, F., Li, Z., Dong, X., Chen, C., & Lu, Y. (2022). Single-atom Pt catalysts as oxidase mimic for p-benzoquinone and α-glucosidase activity detection. *Chemical Engineering Journal*, 449, Article 137855. <https://doi.org/10.1016/j.cej.2022.137855>
- Lee, J., Choi, H., Mun, J., Jin, E., Lee, S., Nam, J., Umer, M., Cho, J., Lee, G., & Kwon, Y. (2023). Nanozyme based on porphyrinic metal-organic framework for electrocatalytic CO₂ reduction. *Small Structures*, 4(1), Article 2200087. <https://doi.org/10.1002/ssr.202200087>
- Li, J.-C., Qin, X., Xiao, F., Liang, C., Xu, M., Meng, Y., Sarnello, E., Fang, L., Li, T., & Ding, S. (2021). Highly dispersive cerium atoms on carbon nanowires as oxygen reduction reaction electrocatalysts for Zn-air batteries. *Nano Letters*, 21(10), 4508–4515. <https://doi.org/10.1021/acs.nanolett.1c01493>
- Liu, J. (2017). Catalysis by supported single metal atoms. *ACS Catalysis*, 7(1), 34–59. <https://doi.org/10.1021/acscatal.6b01534>
- Moullick, M., Das, D., Nag, S., Tudu, B., Bandyopadhyay, R., & Roy, R. B. (2023). Molecularily imprinted polymer-based electrode for tannic acid detection in black tea. *IEEE Sensors Journal*, 23(6), 5535–5542. <https://doi.org/10.1109/JSEN.2023.3240069>
- Piovesan, J. V., Santana, E. R., & Spinelli, A. (2020). A carbon paste electrode improved with poly (ethylene glycol) for tannic acid surveillance in beer samples. *Food Chemistry*, 326, Article 127055. <https://doi.org/10.1016/j.foodchem.2020.127055>
- Pirmohamed, T., Dowding, J. M., Singh, S., Wasserman, B., Heckert, E., Karakoti, A. S., ... Self, W. T. (2010). Nanoceria exhibit redox state-dependent catalase mimetic activity. *Chemical Communications*, 46(16), 2736–2738. <https://doi.org/10.1039/b922024k>
- Qin, W., Su, L., Yang, C., Ma, Y., Zhang, H., & Chen, X. (2014). Colorimetric detection of sulfite in foods by a TMB-O₂-Co₃O₄ nanoparticles detection system. *Journal of Agricultural and Food Chemistry*, 62(25), 5827–5834. <https://doi.org/10.1021/jf500950p>
- Rodríguez, H., de Las Rivas, B., Gómez-Cordovés, C., & Muñoz, R. (2008). Degradation of tannic acid by cell-free extracts of lactobacillus plantarum. *Food Chemistry*, 107(2), 664–670. <https://doi.org/10.1016/j.foodchem.2007.08.063>
- Shan, Y., Liu, Y., Li, Y., & Yang, W. (2020). A review on application of cerium-based oxides in gaseous pollutant purification. *Separation and Purification Technology*, 250, Article 117181. <https://doi.org/10.1016/j.seppur.2020.117181>
- Song, G., Zhang, J., Huang, H., Wang, X., He, X., Luo, Y., Li, J.-C., Huang, K., & Cheng, N. (2022). Single-atom Ce-NC nanozyme bioactive paper with a 3D-printed platform for rapid detection of organophosphorus and carbamate pesticide residues. *Food Chemistry*, 387, Article 132896. <https://doi.org/10.1016/j.foodchem.2022.132896>
- Wang, L., Ge, S., Gao, C., Yan, H., Wang, J., Jia, J., & Wu, Q. (2023). One-pot synthesis of gold-copper nanoparticles mediated by silk fibroin peptides: Peroxidase-like properties and its application in antioxidant detection. *Microchemical Journal*, 185, Article 108250. <https://doi.org/10.1016/j.microc.2022.108250>
- Wang, X., Liu, H., Qiao, C., Ma, Y., Luo, H., Hou, C., & Huo, D. (2024). A dual-functional single-atom Fe nanozyme-based sensitive colorimetric sensor for tannins quantification in brandy. *Food Chemistry*, 434, Article 137523. <https://doi.org/10.1016/j.foodchem.2023.137523>
- Wang, Y., Zhang, Z., Jia, G., Zheng, L., Zhao, J., & Cui, X. (2019). Elucidating the mechanism of the structure-dependent enzymatic activity of Fe-N/C oxidase mimics. *Chemical Communications*, 55(36), 5271–5274. <https://doi.org/10.1039/c9cc01503e>
- Wu, W., Huang, L., Zhu, X., Chen, J., Chao, D., Li, M., Wu, S., & Dong, S. (2022). Reversible inhibition of the oxidase-like activity of Fe single-atom nanozymes for drug detection. *Chemical Science*, 13(16), 4566–4572. <https://doi.org/10.1039/d2sc00212d>
- Wu, Y., Jiao, L., Luo, X., Xu, W., Wei, X., Wang, H., ... Du, D. (2019). Oxidase-like Fe-N-C single-atom nanozymes for the detection of acetylcholinesterase activity. *Small*, 15 (43), Article 1903108. <https://doi.org/10.1002/sml.201903108>
- Xia, Y., He, J., Tang, L., Hu, M., Zhou, J., Xiao, Y.-Y., Jiang, Z.-C., & Jiang, X. (2024). Multifunctional bimetallic MOF with oxygen vacancy synthesized by micropore plasma for rapid total antioxidant capacity assessment in agricultural products. *Food Chemistry: X*, 21, Article 101247. <https://doi.org/10.1016/j.fochx.2024.101247>
- Xie, X., Chen, X., Wang, Y., Zhang, M., Fan, Y., & Yang, X. (2023). High-loading cu single-atom nanozymes supported by carbon nitride with peroxidase-like activity for the colorimetric detection of tannic acid. *Talanta*, 257, Article 124387. <https://doi.org/10.1016/j.talanta.2023.124387>

- Xie, X., Wang, Y., Zhou, X., Chen, J., Wang, M., & Su, X. (2021). Fe–N–C single-atom nanozymes with peroxidase-like activity for the detection of alkaline phosphatase. *Analyst*, *146*(3), 896–903. <https://doi.org/10.1039/d0an01846e>
- Yang, W., Wang, X., Song, S., & Zhang, H. (2019). Syntheses and applications of noble-metal-free CeO₂-based mixed-oxide nanocatalysts. *Chem*, *5*(7), 1743–1774. <https://doi.org/10.1016/j.chempr.2019.04.009>
- Yang, X., Wang, A., Qiao, B., Li, J., Liu, J., & Zhang, T. (2013). Single-atom catalysts: A new frontier in heterogeneous catalysis. *Accounts of Chemical Research*, *46*(8), 1740–1748. <https://doi.org/10.1021/ar300361m>
- Yu, K., Li, M., Chai, H., Liu, Q., Hai, X., Tian, M., Qu, L., Xu, T., Zhang, G., & Zhang, X. (2023). MOF-818 nanozyme-based colorimetric and electrochemical dual-mode smartphone sensing platform for in situ detection of H₂O₂ and H₂S released from living cells. *Chemical Engineering Journal*, *451*, Article 138321. <https://doi.org/10.1016/j.cej.2022.138321>
- Zhang, H., Hwang, S., Wang, M., Feng, Z., Karakalos, S., Luo, L., Qiao, Z., Xie, X., Wang, C., & Su, D. (2017). Single atomic iron catalysts for oxygen reduction in acidic media: Particle size control and thermal activation. *Journal of the American Chemical Society*, *139*(40), 14143–14149. <https://doi.org/10.1021/jacs.7b06514>
- Zhao, M., Yang, R., Wei, Y., Su, J., Wang, X., Zhang, N., Sun, P., Chen, D., & Zhao, Y. (2022). Dual isolated bimetal single-atom catalysts for tumor ROS cycle and parallel catalytic therapy. *Nano Today*, *44*, Article 101493. <https://doi.org/10.1016/j.nantod.2022.101493>
- Zhao, Y., Watanabe, K., & Hashimoto, K. (2012). Self-supporting oxygen reduction electrocatalysts made from a nitrogen-rich network polymer. *Journal of the American Chemical Society*, *134*(48), 19528–19531. <https://doi.org/10.1021/ja3085934>